Computer-Aided Design and Experimental Application of a Novel Electrochemical Cell: The Confluence Reactor

Qiu Fulian,† Nicholas P. C. Stevens,‡ and Adrian C. Fisher*

School of Chemistry, University of Bath, Claverton Down, Bath BA2 7AY, United Kingdom

Received: December 11, 1997; In Final Form: February 24, 1998

A new electrochemical device is reported based on the confluence of two streams of solution. This confluence reactor was designed using finite element simulations to establish the cell geometry and solution velocities appropriate to maintain well-defined hydrodynamic conditions. Computational data is presented to illustrate the flexibility of the tool for the investigation of chemical reaction mechanisms. Experimental studies are presented which examine the relationship between reactant solution velocities and electrolysis current. Excellent agreement is noted between the computational predictions and experimental results. The confluence reactor is shown to be an easy-to-construct, cheap, and simple tool that will offer significant benefits to the exploration of chemical and electrochemical processes. The potential applications of the reactor are noted.

Introduction

Hydrodynamic devices have been employed for an enormous variety of applications in recent years, including mechanistic investigations and analytical detection.[1−5] In the field of electrochemistry, tools such as the rotating disc,[6] channel,[1] and wall-jet electrodes[3] have provided key insights into properties such as the composition and chemical and photochemical reactivity of molecules in fluid solution.[7,8] However, despite their undoubted success, these hydrodynamic tools share a number of common limitations. One of the most significant of these is the inability to mix reagents in a well-defined way close to the detector. In many cases the various reactants are held within the same holding vessel, which severely limits the application of these techniques to the study of rapid chemical reactions. Experimentally it would be desirable to establish a tool that retains the significant versatility of these hydrodynamic devices while enabling the reactants to be held apart from one another until some desired position. In this paper we present a novel hydrodynamic technique that addresses this issue.

The confluence reactor (Figure 1) brings two separate streams of reactants together at a predetermined position under controlled mass transport conditions. The two inlets of the cell are designed so that a parabolic laminar flow profile is established within them, before the two streams meet. Once the streams have converged, the reactant solutions mix and electrochemical detection of the resulting processes is performed approximately 1 cm downstream of the convergence point. This whole process is performed under well-defined mass transport conditions and is therefore quantifiable using appropriate computational models.

To design such a potentially complex tool we have exploited our recently developed finite element packages.[9−11] These enable both convective and diffusive properties of systems to be examined. The simulations enabled the sensitivity and geometry of the proposed cell to be optimized before experimental investigations were undertaken. This computer-aided design approach has allowed experimental studies to focus on feasible geometries without the need for wasteful preliminary investigations.

* Corresponding author. Tel: 44-1225-826 627. Fax: 44-1225-826 231. E-mail: A.C.Fisher@bath.ac.uk.
† E-mail: chpfq@bath.ac.uk.
‡ E-mail: N.P.C.Stevens@bath.ac.uk.

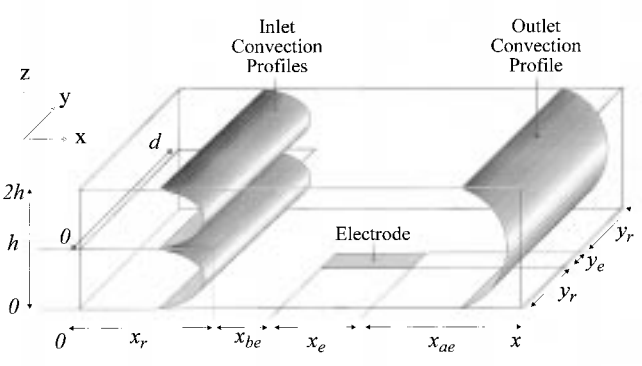

Figure 1. Schematic of a confluence reactor, showing two inlets separated by a thin plate and the electrode (not to scale).

In this cell geometry, computational simulation results and experimental data are all noted for the new cell. Specifically our studies focus on the variation of electrolysis current as a function of the volume flow rate/diffusion coefficients and relative reactant concentrations within the outlets. Excellent agreement is found between experimental and computational predictions. Consequently, the confluence reactor is proposed as a novel hydrodynamic device suitable for mechanistic, kinetic and analytical analysis.

Theory

The confluence reactor design shown in Figure 1 comprises two rectangular inlets separated by a thin aluminum plate, at the end of which forms a larger outlet, passing over a wall-mounted electrode. The behavior of this design was investigated using the simple one electron-transfer reaction

$$A + e^- \rightarrow B$$

The confluence reactor may be modeled in two dimensions, neglecting the *y* direction, as shown in Figure 1. This assumption is commonly made in the simulation of channel electrode geometries and is valid, provided that the electrode is centrally placed in the *y* direction, allowing the flow profile to be approximately uniform along this axis. The steady-state mass transport for a system of this type is given by

$$D\frac{\partial^2 C}{\partial x^2} + D\frac{\partial^2 C}{\partial z^2} - V_x\frac{\partial C}{\partial x} - V_z\frac{\partial C}{\partial z} = 0 \qquad (1)$$

S1089-5647(98)00500-8 CCC: $15.00
Published on Web 04/22/1998

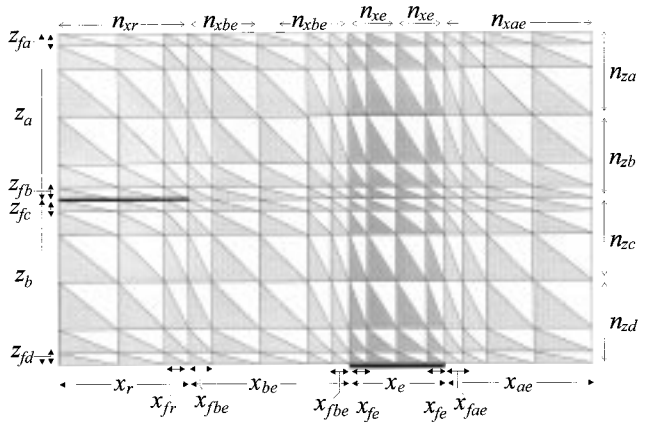

Figure 2. Schematic of the grid of finite elements used for solution of the confluence reactor concentration profile.

where D is the diffusion coefficient, C is the concentration of the species under study, and and V_x and V_z are the velocities in the directions defined in Figure 1.

In this paper we report initial investigations for this geometry employing macroelectrodes of size $x_e \approx 0.6$ cm and $y_e \approx 0.42$ cm, in cells where $h = 0.04$ cm.

Matrix Formation

The finite element method is employed to solve eq 1 over the domain of interest. The region under study is discretized into an assembly of elements using the Galerkin finite element formulation, as discussed previously. A matrix equation is then formed from a summation of the contributions from each element, the solution of which satisfies eq 1. This is

$$[K]\vec{C} = 0$$

where the characteristic matrix is found as

$$[K] = \frac{D}{4A^{(e)}}\begin{bmatrix} b_i^2 + c_i^2 & b_ib_j + c_ic_j & b_ib_k + c_ic_k \\ b_ib_j + c_ic_j & b_j^2 + c_j^2 & b_jb_k + c_jc_k \\ b_ib_k + c_ic_k & b_jb_k + c_jc_k & b_k^2 + c_k^2 \end{bmatrix} - \frac{V_x}{6}\begin{bmatrix} b_i & b_j & b_k \\ b_i & b_j & b_k \\ b_i & b_j & b_k \end{bmatrix} - \frac{V_z}{6}\begin{bmatrix} c_i & c_j & c_k \\ c_i & c_j & c_k \\ c_i & c_j & c_k \end{bmatrix}$$

where D is the diffusion coefficient of the species in question, $A^{(e)}$ is the area of the element, V_x and V_z are the velocities in x and z, and the variables b_{i-k} and c_{i-k} are derived from the nodal coordinates of each element as given below where x_i is the x coordinate of point i, z_j is the z coordinate of point j of the triangular element in question, and so on.

$$b_i = z_j - z_k \qquad b_k = z_i - z_j \qquad c_j = x_i - x_k$$
$$b_j = z_k - z_i \qquad c_i = x_k - \mathrm{xj} \qquad c_k = x_j - x_i$$

Element Grid Formation

The region under investigation must be considered as a tessellation of elements covering the cell. The grid can be nonuniform, and it is found that concentrating the elements in regions of high flux gives the most computationally efficient method. Figure 2 shows a schematic of the grid and typical parameters used in this paper. Parameters of the form z or x indicate dimensions of the cell and parameters of the form n denote the number of finite elements across a region, with the subscript denoting the region described. An f subscript denotes the size of the first element over a section of the grid, which along with the total number of elements across the section and the total size define a geometric series for the sizes of the other elements.

Boundary Conditions

The boundary conditions appropriate to the problem of interest are

$z = 0$	$x < x_r + x_{be}$	$dC/dz = 0$
$z = 0$	$x_r + x_{be} < x < x_r + x_{be} + x_e$	$C = 0$
$z = 0$	$x > x_r + x_{be} + x_e$	$dC/dz = 0$
$z = h$	$x < x_r$	$dC/dz = 0$
$z = 2h$	all x	$dC/dz = 0$
all z	$x = 0$	$C = C_{Bulk}$
all z	$x = x_r + x_{be} + x_e + x_{ae}$	$dC/dx = 0$

Current Calculation

The current flowing at the electrode is determined from the concentration gradient at the electrode. This is provided by the simulation, and the current is then derived as previously detailed by the relation

$$I = FD[C]_{Bulk}\, y_e \sum_{i=1}^{ne} \frac{\delta x_i}{\delta z_i} \sum_{j=1}^{2} \frac{1}{2}[C]_{E(i,j)}$$

where E(ne, 2) is defined to be an array numbering each square pair of triangular elements lying above the electrode surface from 1 to ne and also containing the global numbers of the two nodes at the top edge of this square. δx_i and δz_i are the dimensions of the square, and y_e is the width of the electrode as shown in Figure 1. D is the diffusion coefficient, and $[C_{Bulk}]$ is the bulk concentration of the species under investigation.

Hydrodynamic Simulations

The velocity field over the cell is found by the solution of the Navier Stokes equations by a finite element method.[10] The simultaneous solution of the three equations

$$u'\frac{\partial u'}{\partial x'} + v'\frac{\partial u'}{\partial z'} = \frac{F_x l}{\rho {u_0}^2} - \frac{\partial p'}{\partial x'} + \frac{\nu}{u_0 l}\left(\frac{\partial^2 u'}{\partial x'^2} + \frac{\partial^2 u'}{\partial z'^2}\right)$$

$$u'\frac{\partial v'}{\partial x'} + v'\frac{\partial v'}{\partial z'} = \frac{F_x l}{\rho {u_0}^2} - \frac{\partial p'}{\partial z'} + \frac{\nu}{u_0 l}\left(\frac{\partial^2 v'}{\partial x'^2} + \frac{\partial^2 v'}{\partial z'^2}\right)$$

$$\frac{\partial u'}{\partial x'} + \frac{\partial v'}{\partial z'} = 0$$

where the normalized variables (denoted by primes) are $x' = x/l$, $z' = z/l$, $u' = u/l$, and $p' = \rho u_0^2$, where x and z are the coordinates of the point of interest, u and v the velocities in x and z, and p is the pressure. Also, l is a characteristic length, and u_0 is a specified velocity. The finite element formulation of these equations has been more fully explored previously in the literature.[12]

Experimental Section

A schematic of the confluence reactor is shown in Figure 3 and can be seen to be constructed from two rectangular ducts separated in the nonmixing region with aluminum foil. The two ducts were fabricated from synthetic fused silica (Heraeus silica and Metals Byfleet, Surrey) and cemented together using a low melting point wax.[13] Platinum electrodes of typical dimension 4 mm × 2 mm (Goodfellows Metals Ltd) were employed for electrochemical detection. The electrode was cemented onto one face of the cell and polished to 0.25 μm smoothness using progressively decreasing sizes of diamond

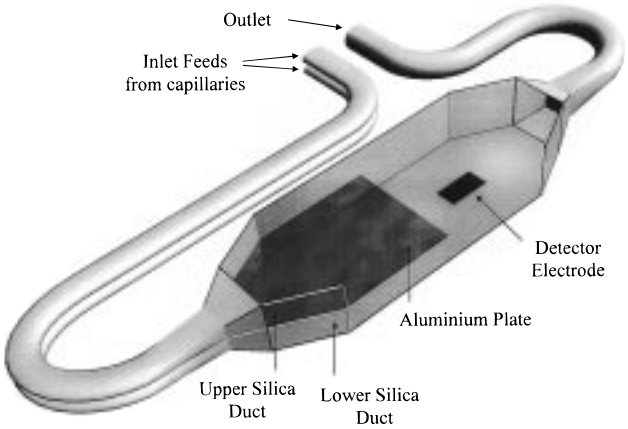

Figure 3. The confluence reactor.

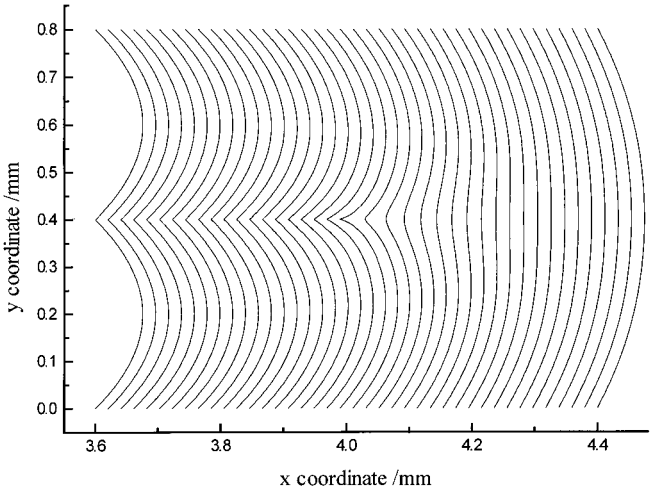

Figure 4. Flow lines through the confluence reactor.

lapping compound. Electrical contact was made to the electrode via a small hole in the cell which was sealed using epoxy resin. A fully constructed cell had typical internal dimensions of height 0.08 cm, width 0.6 cm, and length 2.5 cm.

The confluence reactor was held in a gravity fed flow system, the essential details of which have been noted previously.[13] Two separate reservoirs were employed to hold the appropriate electrolyte solutions. The inlet solution flow rates were controlled by the use of two capillaries placed upstream of the reactor which enabled solution flow rates in the range 10^{-3}–10^{-1} cm^3 s^{-1} to be accessed. A silver pseudo-reference wire was also placed upstream of the cell. A platinum gauze counter electrode 80 mm × 30 mm (52 mesh) was located downstream of the reactor to ensure counterproducts did not enter the reaction vessel. The apparatus was prepared for the experiment by flushing degassed argon solvent through the system which acted to remove any oxygen.

Electrolyte solutions were prepared using acetonitrile (Fisons) dried over alumina and distilled. Tetrabutylammonium perchlorate, TBAP (Fluka, purum), was employed as background electrolyte (typically 0.1 mol dm^{-3} concentration). Tris-bromophenylamine (TBPA) (Aldrich) and ferrocene (Aldrich) were used as received.

Results and Discussion

Theoretical Discussion. Initial simulations were performed to optimize the design of the confluence reactor for the experimental investigations. Figure 4 shows a set of flow lines generated as part of this process for a reactor of geometry $z_a =$

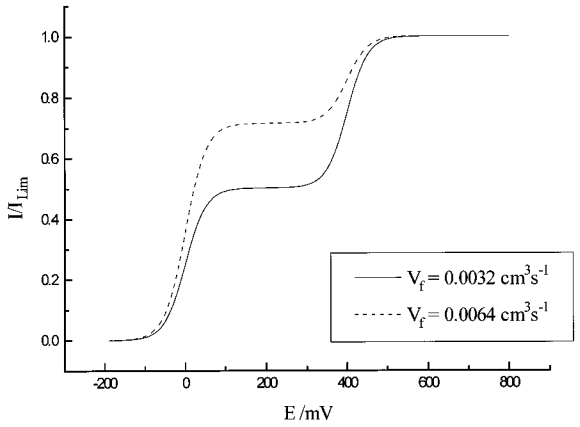

Figure 5. Current voltage plot at two flow rates for the confluence reactor.

$z_b = 0.04$ cm at $V_f = 0.009\,72$ cm^3 s^{-1}. These contours show the velocity profile over the region 0.4 mm either side of the end of the central aluminum plate, showing the rapid transition from the two parabolic profiles of the inlets to the larger parabola in the outlet.

The confluence reactor offers the possibility of mixing two streams of material, under very well-defined conditions. Perhaps the simplest example of this is the case when one inlet contains reactant, in solution with a suitable background electrolyte, and the other contains only the background electrolyte. At very low flow rates the concentration profile of the species in solution becomes uniform in z before the electrode is reached. Under these conditions the response seen at the electrode is the same whether the reactant is introduced through the upper or lower inlet and may be approximately predicted using the Levich equation.

Preliminary simulations were performed for various geometries and flow rates. At very low flow rates the confluence reactor behaves as an analogue of a channel cell of height $2h$. This situation changes as the flow rate is increased. A point is reached where the concentration profile does not become uniform in z before the electrode is reached. If the reactant is introduced through the lower inlet, the predicted current at the electrode tends to the Levich response for a channel of height h. If the reactant is introduced through the upper inlet, the current tends to zero as the flow rate rises, as in the case for the opposite-sided double-electrode cell, as the electroactive species is carried past the electrode before diffusion can carry it across the cell to the electrode.

Figure 5 shows two simulated steady-state current/voltage plots for the confluence reactor, showing the divergence in the response between two species introduced through the top and bottom channels as the flow rate is increased, where I_{Lim} is the mass transport limited current. The value of E_0 for the species introduced through the bottom inlet is set to zero, and that for the species flowing in through the top inlet is set to +400 mV. The parameters used were as given in the description of below Figure 10.

Sample concentration profiles may also be examined to illustrate the effect of increased convection. Figure 6 shows two typical concentration profiles, at different flow rates, under conditions where no electrode reaction occurs.

The effect of the increased convection in lengthening the distance necessary for the concentration profile to approach uniformity in the z direction is obvious.

This new geometry is also found to be sensitive to the diffusion coefficient of the species. Figure 7 shows the effect

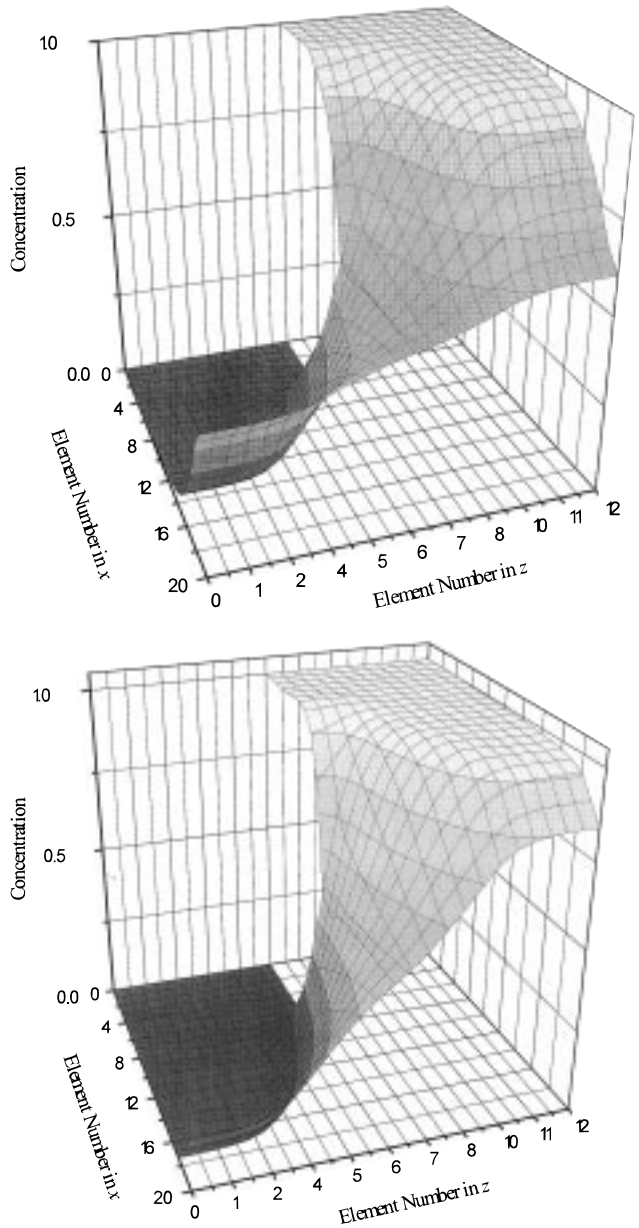

Figure 6. Concentration profiles in the confluence reactor at a low flow rate (a, top) and a high flow rate (b, bottom).

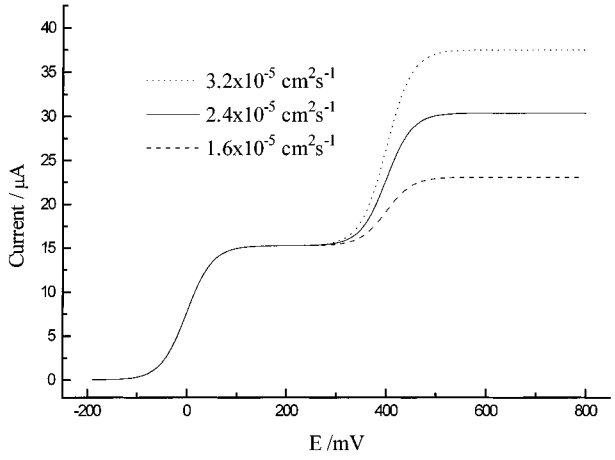

Figure 7. Current voltage plots showing the effect of varying diffusion coefficients.

of varying the diffusion coefficient of the species introduced through the top channel, using the same parameters as for the results in Figure 5, but with the diffusion coefficients shown, and $V_f = 0.0032$ cm^3 s^{-1} in all three cases.

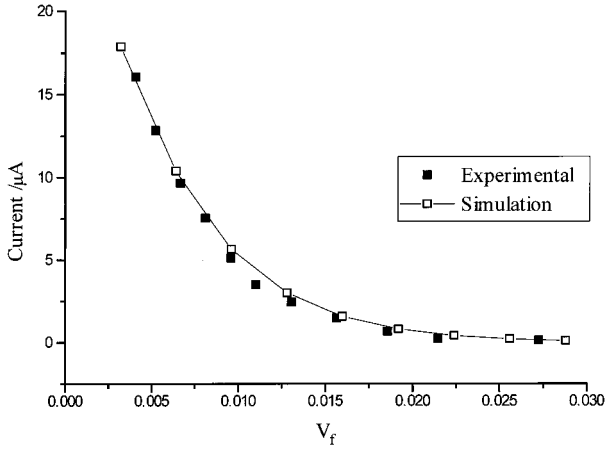

Figure 8. Results and simulation for mode 2 operation.

From the simulation data available, for every combination of geometry and diffusion coefficient, the range of flow rates over which the response at the electrode will vary most strongly is found, and from these possible sets of parameters, those that are most suited to experimental application were chosen. Initial simulations showed that a gap between the junction of the two inlets and the electrode needed to be greater than 1 cm for an appreciable current to be measured at the electrode when the electroactive species was introduced through the upper channel, at flow rates sufficiently high as to be experimentally practical.

Experimental Discussion

To evaluate the new arrangement, experiments were performed using various different operating modes. In the first set of measurements (mode 1) a single reactant tris(*p*-bromophenyl)amine[14] (TBPA) of the same concentration is placed in both reservoirs. Typical conditions employed were 1.1 mmol TBPA and 0.1 M tetrabutylammonium perchlorate (TBAP) acetonitrile solutions with cell parameters of $d = 0.6$ cm, $h = 0.041$ cm, $x_{be} = 1.22$ cm, $x_e = 0.419$ cm, and $x_{ae} = 0.2$ cm. The mass transport limited current from the oxidation of TBPA to the corresponding cation was then recorded as a function of the volume flow rate. For all measurements undertaken both inlets were fixed at the same volume flow rate. Using mode 1 the results were in excellent agreement with the predicted values using the Levich equation for a channel cell[15] with a bulk solution concentration of 1.1 mmol. This can be rationalized since under the experimental conditions of operation the length of cell required after the inlet region to reestablish fully parabolic flow is of the order of 1 mm. The supply of the same material from each of the outlets simply results in an experiment essentially identical to those reported previously for the channel flow cell[1].

Next experiments were performed with only one of the inlets containing the electroactive material, 2mM ferrocene,[16] which we shall refer to as mode 2. Figure 8 shows typical experimental results along with values predicted using the numerical calculations for the case where material is introduced from the outlet on the far side of the cell relative to the electrode. All parameters were as for Figure 10 except $d = 0.42$ cm.

As can be seen, the current drops as a function of increasing volume flow rate. This can be explained since the transit time of material in the cell must be comparable to the time taken for material to diffuse across the cell and be detected. As the flow rate is increased the current therefore gradually drops,

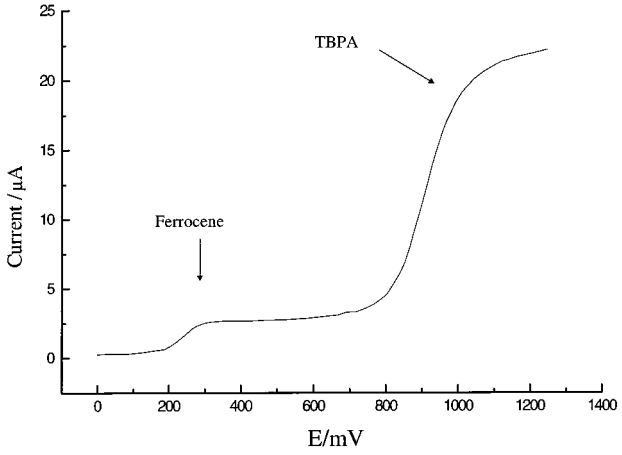

Figure 9. Experimental current/voltage plot for mode 3 operation.

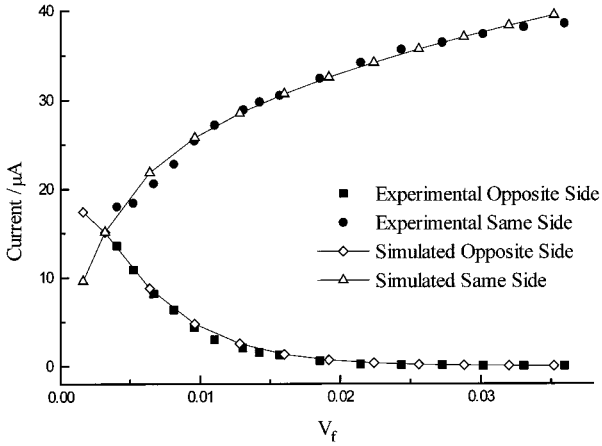

Figure 10. Results and simulation for mode 3 operation.

reflecting the fact that less material is able to diffuse over from the far side of the cell. The opposite is true when material is allowed to enter from the bottom inlet only. The upper line in Figure 10 shows this case for both experimental and theory values of a 1.0 mmol TBPA solution. Now as the flow rate increases the detected current also rises. Of course this is a result of the material now staying closer to the wall in which the detector is mounted. At sufficiently high flow rates, the current response becomes identical to that of the a cell operated in mode 1, since the concentration near the surface is effectively the same as that leaving the bottom inlet.

The final mode (3) of operation examined in this paper is the case where different reactants are introduced from the two inlets. In mode 3 two electrochemically well-defined materials, TBPA as above and ferrocene were examined. Acetonitrile solutions of TBPA and 2.0 mmol ferrocene, both containing 0.1 M TBAP, were degassed in separate reservoirs. The experiments were performed with both outlets fixed at the same flow rate, and a steady-state voltammogram was then recorded. Figure 9 shows a typical voltammogram recorded using at. 0.43 mmol TBPA and 11 mmol ferrocene.

The two materials can be seen clearly as separate waves on the voltammogram. This procedure was repeated for a range of volume flow rates. A typical set of experimental results obtained for the variation of the mass transport limited current as a function of the volume flow rate are noted in Figure 10 for 1.0 mmol TBPA in the adjacent channel and 2.0 mmol ferrocene in the opposite channel. Again numerical results are also presented, and it is apparent that excellent agreement is noted between the experimental and computational predictions. The parameters used were $x_r = 0.4$ cm, $x_{be} = 1.22$ cm, $x_e = 0.419$ cm, $y_e = 0.355$ cm, $d = 0.6$ cm, $x_{ae} = 0.2$ cm, $z_a = 0.04$ cm, $z_b = 0.04$ cm, $n_{xr} = 10$, $n_{xbe} = 10$, $n_{xe} = 10$, $n_{xae} = 10$, $n_{ya} = 10$, $n_{yb} = 10$, $n_{yc} = 10$, $n_{yd} = 12$.

Conclusion

The confluence reactor has been shown to be of great interest as a novel cell geometry allowing rapid mixing of materials under precisely defined hydrodynamic conditions. The simulation of the behavior of the device has allowed both rapid development of this system and verification of the experimental results obtained. Future applications of this geometry are many, and further work may easily include applications in kinetic resolution and photoelectrochemistry.

Acknowledgment. We thank the EPSRC for studentship 957 00 361 for N.S., Bath University for support for Q.F., and the Nuffield Foundation for supporting this research.

References and Notes

(1) Compton, R. G.; Unwin, P. R. *J. Electroanal. Chem.* **1986**, *206*, 57.
(2) Anderson, J. L.; Moldoveanu, S. *J. Electroanal. Chem.* **1984**, *179*, 107; 119.
(3) Glauert, M. B. *J. Fluid Mech.* **1956**, *1*, 625.
(4) Compton, R. G.; Coles, B. A.; Fisher, A. C. *J. Phys. Chem.* **1994**, *98*, 2441.
(5) Aixill, W. J.; Fisher, A. C.; Fulian, Q. *J. Phys. Chem.* **1996**, *100*, 14067−14073.
(6) Riddiford, A. C. *Adv. Electrochem. Eng.* **1966**, *4*, 47.
(7) Compton, R. G.; Coles, B. A.; Gooding, J. J.; Fisher, A. C.; Cox, T. I. *J. Phys. Chem.* **1994**, *98*, 2446.
(8) Compton, R. G.; Fisher, A. C.; Wellington, R. G., Bethell, D.; Lederer, P. *J. Phys. Chem.* **1991**, *95*, 4749.
(9) Stevens, N. P. C.; Hickey, S. J.; Fisher, A. C. *J. Ann. Quim.* **1997**, *93*, 225−232.
(10) Stevens, N. P. C.; Fisher, A. C. *J. Phys Chem.* **1997**, *101*, 8259−8263.
(11) Stevens, N. P. C.; Fisher, A. C. *J. Electroanal. Chem.*, in press.
(12) Taylor, C.; Hughes, T. G. *Finite Element Programming of the Navier−Stokes Equations*, 1st ed.; Pineridge Press: Swansea, 1981.
(13) Compton, R. G.; Unwin, P. R. *J Electroanal. Chem.* **1986**, *205*, 1.
(14) Barton, D. H. R.; Haynes, R. K.; Leclerc, G.; Magnus, P. D.; Menzies, I. D. *J. Chem. Soc., Perkin Trans. 1* **1975**, 2055.
(15) Unwin, P. R.; Compton, R. G., *Compr. Chem. Kinet.* **1989**, *29*, 193.
(16) Peover, M. J. *J. Chem. Soc.* **1962**, 4540.